Inversion of data for near-grazing propagation over graveled surfaces

R. J. Lucas[a] and V. Twersky
Mathematics Department, University of Illinois, Chicago, Illinois 60680

(Received 15 September 1986; accepted for publication 19 November 1986)

Data obtained by Medwin and D'Spain [J. Acoust. Soc. Am. 79, 657 (1986)] for low-frequency propagation over gravel-covered rigid planes are inverted by applying the procedure [J. Acoust. Soc. Am. Suppl. 1 79, S68 (1986)] developed for regularly shaped protuberances. The development is based on analytical results for a point source irradiating an embossed plane, and on the uniform asymptotic form of the coherent field as a Sommerfeld type wave system in terms of the complex error function complement (Q). Initial estimates of unknown parameters are obtained by working with elementary approximations of the Q integral, and then used in the complete integral for refinements and final computations. The procedure delineates the roles of interference and damping on the elementary wave components of the Q system, and the resulting graphs display the primary data trends.

PACS numbers: 43.20.Fn, 43.20.Bi, 43.30.Gv

INTRODUCTION

An earlier article[1] applied analytical results[2] for the coherent response to a point source irradiating an embossed rigid plane to interpret and invert data[3] for low-frequency (small k) propagation over periodic or densely packed distributions of regularly shaped protuberances. The present article applies the same data inversion procedure to recent measurements by Medwin and D'Spain[4] for a monolayer of fine gravel ($\equiv$1, aquarium type) covering a rigid plane. The results delineate the roles of interference and damping on the elementary components of the Sommerfeld type uniform asymptotic representation[2] in terms of the complex error function complement (Q). As before, we obtain initial estimates of unknown parameters in the surface impedance ($\zeta = i\xi - \eta$) by using elementary approximations for the Q integral, and then use the complete integral for refinements and final computations [based on International Mathematical and Statistical Routines Library (IMSL) subroutine MERRC2].

As for the densely packed monolayer of spheres on a plane,[1,5] we find that the $O(k)$ term of ξ has to be supplemented by a k^{-1} term, and that η is $O(k)$ corresponding to an effective loss with negligible incoherent scattering (which would require a k^{-1} dependence[5,6]). We obtain initial estimates from some of the data for one set of magnitudes (S) vs k, and use remaining S data and incremental dispersion (I) data for substantiation, and then demonstrate that resulting curves for the normalized power P (vs k, range, and height) are consistent with primary data trends. As before for spheres,[5] the damped oscillatory behavior of S data records[4] with increasing k substantiates the original[2] prediction of the interference effects of the Sommerfeld type wave components, and emphasizes the inadequacies of a Zenneck type wave or its radially damped modifications.[7,8] The extrema (S_n) of S and the corresponding frequencies (k_n) are key to the data reduction. Although the values used for the surface parameters, and for the locations of the phase centers of the transducers, are not necessarily optimal, they suffice for primary data trends. In the following, for brevity, we use (2:18) for Eq. (18) of Ref. 2, and Fig. 4:1 for Fig. 1 of Ref. 4, etc., and the same notation as before.[1]

I. KEY FORMS

We write the total field as

$$\Psi = \Phi + U = \Phi P e^{i\eta} = \Phi(1 + Se^{i\sigma}), \tag{1}$$

where (P,S,φ,σ) represent Medwin's (P_R/P_D, P_R/P_D, ϕ_{RD}, ϕ_{RD}), and Φ is the sum of the source wave and its image $E(r) = e^{ikr}/r$ in the base plane. We use $r = (z^2 + \rho^2)^{1/2}$, $\theta = \pi/2 - \tau$, $\tan\tau = z/\rho$, such that $z = h_t + h_r$ is the sum of the heights of the phase centers of the transmitter and receiver above the base plane, and ρ is the separation of the projections of the centers on the base. The normalized phase difference

$$I = [\varphi(\rho_2) - \varphi(\rho_1)]/k(\rho_2 - \rho_1), \quad \rho_2 > \rho_1, \tag{2}$$

corresponds to Medwin's incremental dispersion.

The field depends on the plane-wave reflection impedance

$$\zeta(\theta) = i\xi(\theta) - \eta(\theta), \tag{3}$$

whose critical value

$$\cos\bar{\alpha} = \zeta(\bar{\alpha}) = \bar{\zeta} = i\bar{\xi} - \bar{\eta}, \quad \bar{\xi} \gg \bar{\eta} \geq 0 \tag{4}$$

determines the Sommerfeld parameter $s^2 = kr[\cos(\theta - \bar{\alpha}) - 1]$. From (2:18),

$$U \sim \frac{2\zeta(\theta)E(r)}{\cos\theta - \zeta(\theta)} - ik\Gamma e^{ikr}\left(\frac{2}{\pi kr}\right)^{1/2}\left(\frac{\sqrt{\pi}}{s} + e^{i(s^2 - \pi/4)}Q(s)\right),$$

$$Q(s) = \pi i + 2\sqrt{\pi}ie^{i\pi/4}\int_0^s e^{-it^2}\,dt, \tag{5}$$

[a] Visiting from the Department of Mathematical Sciences, Loyola University, Chicago, IL.

 0001-4966/87/030619-05$00.80

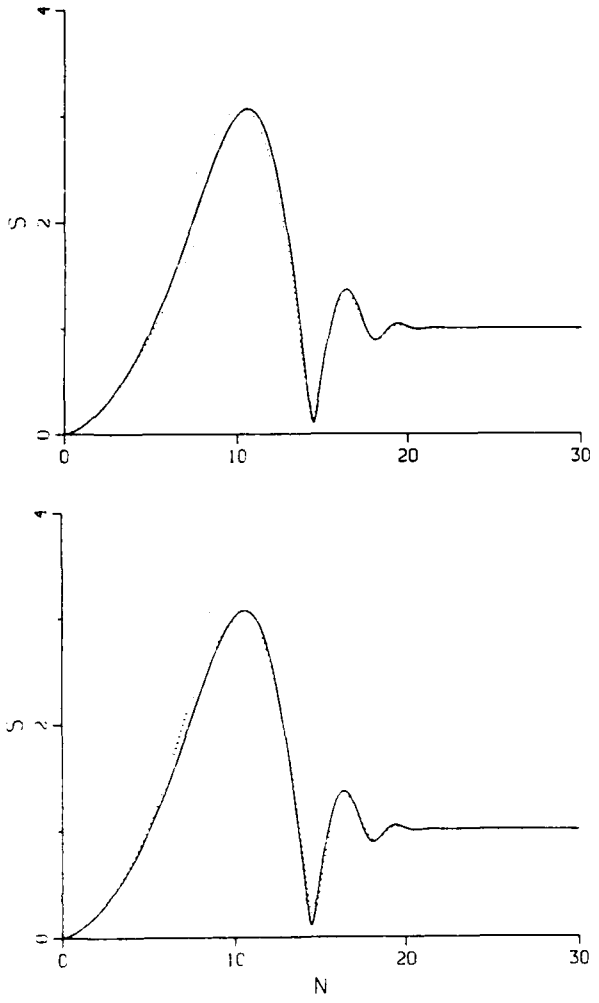

FIG. 1. Magnitude S in (1) vs N in kHz at range $\rho = 320$. The parameters are as in (17) for all figures, and $h_r = h_s = 0.835$ for Figs. 1–7. The solid curve is based on (5), and the dotted curves (that equal the solid at large and small N) are the large and small s approximations (8) and (11) with $\bar{\zeta}' = 0$ (top), or (10) and (12) (bottom).

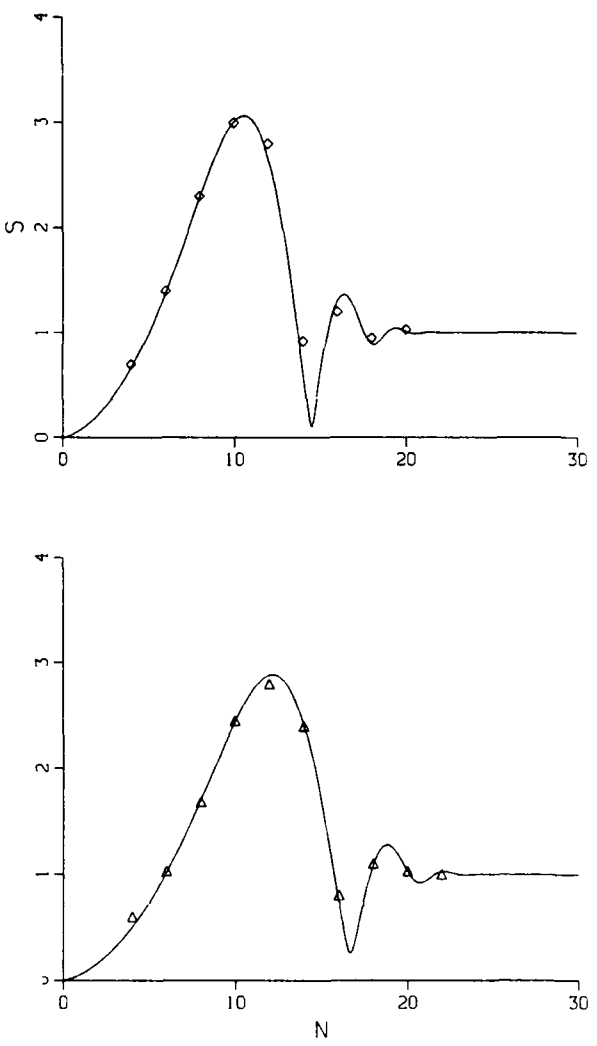

FIG. 3. The S curves for $\rho = 320$ (top) and 200 (bottom) compared with Fig. 4:1 data.

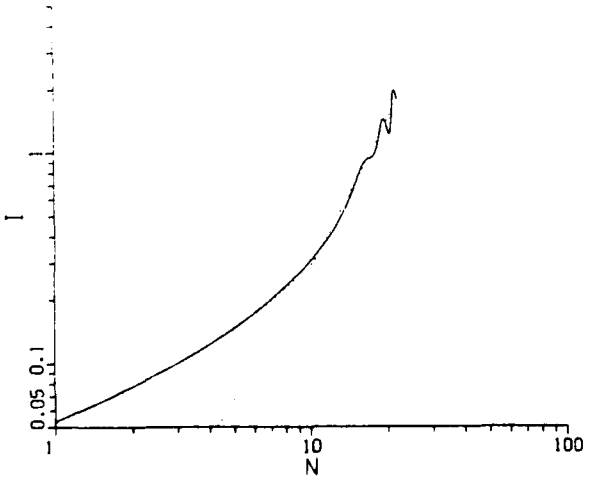

FIG. 2. Incremental dispersion I of (2) in percent between $\rho_2 = 320$ and $\rho_1 = 260$. The solid curve is based on (5) and the dotted curves correspond to (13) and (14).

where $\Gamma = \bar{\zeta}/(\sin\bar{\alpha} + \bar{\zeta}')$ and the prime means differentiate with respect to argument.

For small ζ and τ,

$$s \approx (kr/2)^{1/2}(\bar{\xi} + i\bar{\eta} + i\tau) = s_r(1 + i\epsilon)\,,$$
$$s_r = (kr/2)^{1/2}\bar{\xi}\,, \quad \epsilon = (\bar{\eta} + \tau)/\bar{\xi}\,. \tag{6}$$

Suppressing the argument $\theta = \pi/2$,

$$\bar{\zeta} \approx \zeta(1 - \bar{\zeta}'/2)\,, \quad \zeta = i\xi - \eta\,, \quad \bar{\zeta}' \approx -|\xi\xi''|\,, \tag{7}$$

where the leading term of ξ is $O(k)$ and $\bar{\zeta}'$ is $O(k^{-2})$.

For large s, as in (2:24),

$$Se^{i\sigma}(1 - \tau/\zeta) \sim -1 + [2s\sqrt{\pi}/(1 + \bar{\zeta}')]\, e^{i(s^2 + \pi/4)}\,, \tag{8}$$

with

$$is^2 \approx ik\rho\bar{\xi}^2/2 - k\bar{\xi}z - k\bar{\xi}\bar{\eta}\rho \approx is_r^2 - s_r^2 2\epsilon\,. \tag{9}$$

Initial estimates can be based on the ultra simplified version (1:13),

$$Se^{i\sigma} = -1 + Pe^{i\vartheta} \sim -1 + 2s_r\sqrt{\pi}e^{i(s^2 + \pi/4)}\,, \tag{10}$$

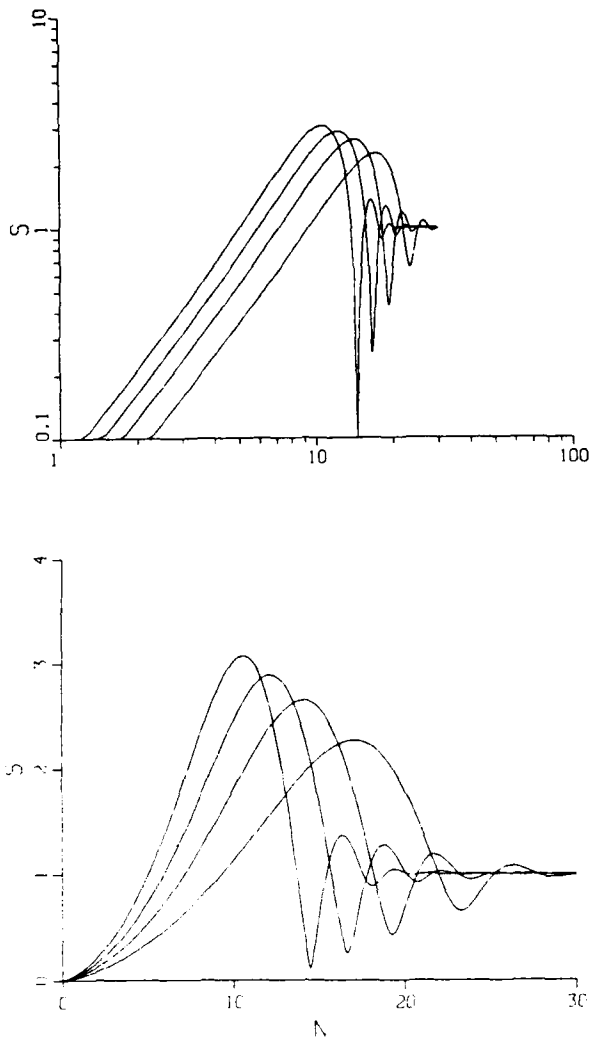

FIG. 4. Overlay of S curves for ρ = (320, 200, 120, 60) corresponding to Fig. 4:1. The curves for the shorter ranges (the lower curves at small N) show less accord with data than Fig. 3 for longer ranges, and may require different values of h_1 and h_2.

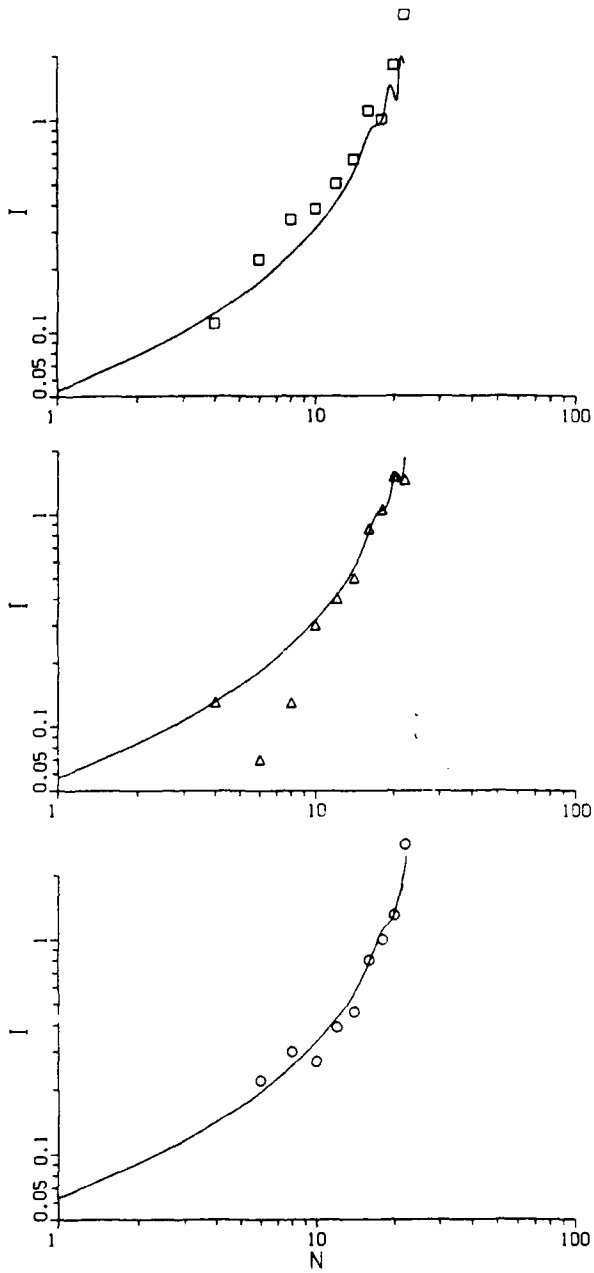

FIG. 5. The I curves compared with Fig. 4:2 data for (ρ_2, ρ_1) = (320, 260) at top, (280, 220) in center, and (240, 180) at bottom.

whose damped oscillatory structure was discussed and graphed earlier in full detail.[1,2] For small s, as in (2:20),

$$Se^{i\sigma}(1-\tau/\xi)(1+\overline{\xi}') \sim -\overline{\xi}' + se^{i(s^2+\pi/4)}(\sqrt{\pi}+2se^{i\pi/4}) . \quad (11)$$

For negligible $\overline{\xi}'$ to lowest order in ϵ,

$$S \approx s\sqrt{\pi} + s^2(1-\epsilon)\sqrt{2} . \quad (12)$$

The correspondi.ig forms of I of (2) follow from (10) and (11). For large s,

$$I \sim [s_r^2(\rho_2) - s_r^2(\rho_1)]/k(\rho_2-\rho_1) = \overline{\xi}^2/2 , \quad (13)$$

and for small s,

$$I \sim \overline{\xi}(1+\epsilon)\sqrt{\pi}/2(\sqrt{\rho_2}+\sqrt{\rho_1})\sqrt{k} + \overline{\xi}^2(1-\pi/4) . \quad (14)$$

For rigid bosses on a rigid base,

$$\xi(\theta) = kV(\delta \sin^2\theta - 1) + O(k^{-1}) , \quad (15)$$
$$\xi = kC(1+\gamma k^{-2}) + O(k^{-5}) , \quad C = V(\delta - 1) .$$

Here, $V = nv/2$ is the volumetric departure from the plane (the raised volume in unit area), v is the volume of a boss plus its image, and n is the number in unit area; δ represents the dipole, -1 the monopole, and γ the leading higher-order corrections. For rigid surfaces, we require $\eta = 0$ for periodic distributions and $\eta = O(k^{-4})$ for incoherent scattering by random distributions of bounded bosses,[5,6] but neither sufficed for Medwin's data.[3,4] To include effective losses, we investigated[1] $\eta = ACk^{\mu}(1+3\gamma k^{-2})$ with $\mu = (1,2,3,4)$, as well as other forms, and found best accord for $\mu = 1$. Thus, as before,[1] final computations are based on

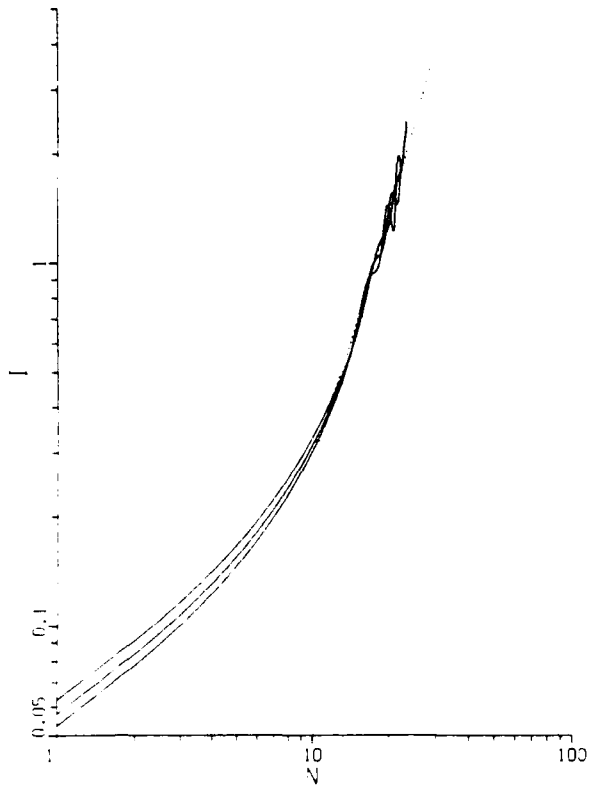

FIG. 6. Overlay of I curves for Fig. 4:2. At small N, the highest corresponds to (240, 180), the middle to (280, 220), and the lowest to (320, 260). The dotted curve is based on the ρ-independent approximation (13).

$$\xi = i\bar{\xi} - \eta\,, \quad \bar{\xi} \simeq kC(1+\gamma k^{-2})\,, \quad \eta \simeq kCA(1+3\gamma k^{-2})\,,$$
$$C = V(\delta - 1)\,, \quad \bar{\bar{\xi}} \simeq \bar{\xi}(1 - \bar{\eta}^2/2) \simeq \bar{\xi}(1+\beta k^{-2})\,, \qquad (16)$$
$$\beta = \delta(\delta-1)V^2\,, \quad \bar{\bar{\xi}} \simeq kC\,[1 + (\gamma+\beta)k^{-2}]\,.$$

For known V, we work with three parameters (CA,γ) and obtain initial estimates from data for the extrema of S and their corresponding values of k by using (10).

II. COMPARISONS WITH DATA

The values of the parameters for the fine gravel (#1, aquarium type) were isolated from Figs. 4:1 and 4:2 by estimations with (10) and substantiations with (12)–(14) were refined by computations with (5). The values used in all graphs are

$$(CA,\gamma) = (4.15, 0.46)\times 10^{-2}\,,$$
$$\delta = 1.39\,, \quad \beta = 5.75\times 10^{-3}\,, \qquad (17)$$

corresponding to the given value[4] $V = 0.103$ cm, and frequencies determined by $N = (k/0.183)$ cm in kHz. All values we use for lengths are in cm, and C is in cm, γ (and β) in cm^2, and A (and δ) are dimensionless.

The ranges of validity in N of the simple analytical approximations we used for initial estimations (based on S) and substantiations (based on I) are shown in Figs. 1 and 2. The accord indicates that the simplified versions may be used for most practical purposes at $\tau \simeq 0$.

Figures 3 and 4 show S data from Fig. 4:1 and theory

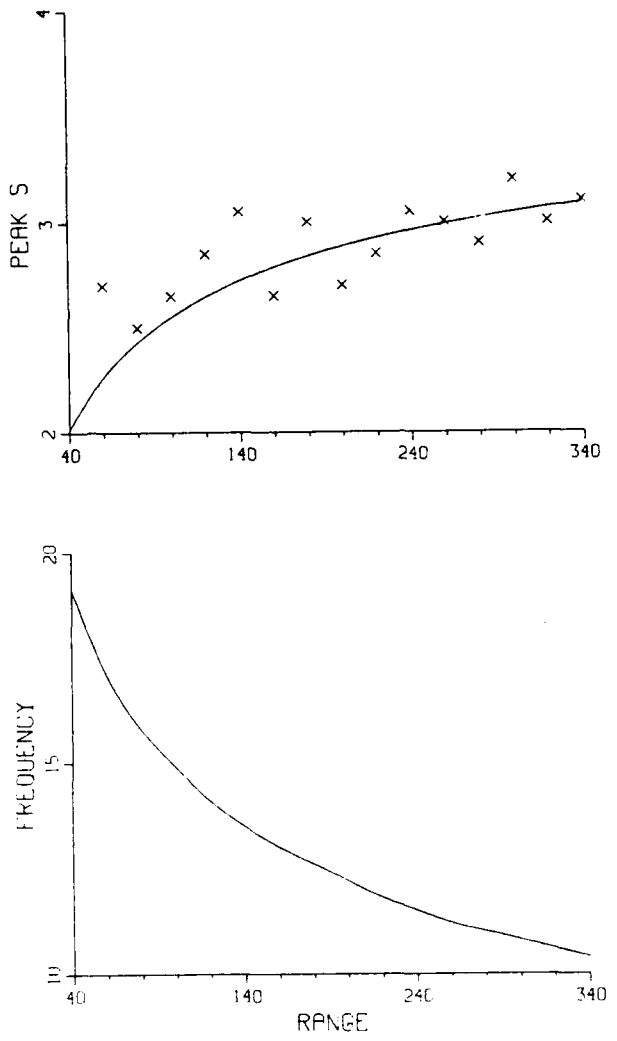

FIG. 7. The peak S_1 (first maximum of S) and the corresponding frequency N_1 vs ρ based on (5) compared with Fig. 4:6 data for #1 gravel.

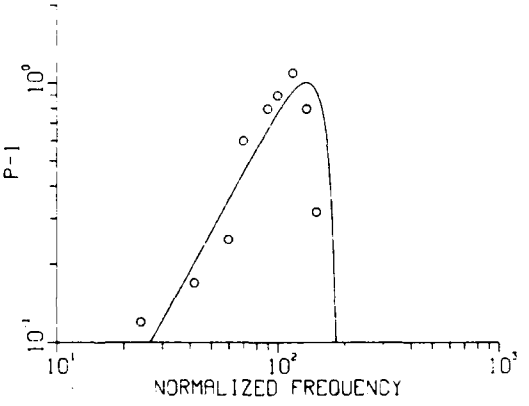

FIG. 8. Curve of $P-1$ of (1) based on (5) for $h_1 = h_2 = 0.3$ compared with Fig. 4.10 data (for #1 gravel, at $Z_1 = Z_2 = 0$ and $\rho = 40$) versus $k\rho = 7.32N$ and N varying from 4 to 20 in steps of 2.

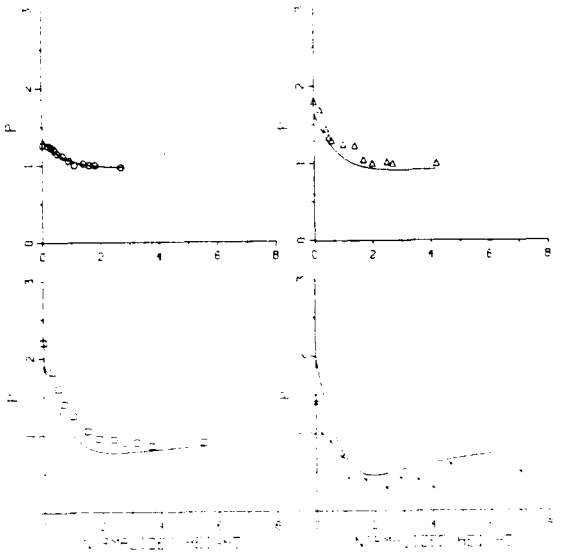

FIG. 9. Curves of P of (1) based on (5) for $h_t = 0.3$ and $h_r > 0.3$ compared with Fig. 4:13 data (at $\rho = 40$, $Z_s = 0$, and $Z_r > 0$) versus $kZ_r/2\pi$; the circles, triangles, squares, and $\times$'s correspond to $k\rho = 58$, 87, 117, and 146 (essentially, $N = 8$, 12, 16, and 20). To include the dominant effect of increasing h_t in $\zeta(\theta)$, we replaced δ in the $O(k)$ term of ζ by $\delta \sin^2 \theta$.

versus N, and Figs. 5 and 6 show I data from Fig. 4:2 and theory versus N. Figure 7 compares data of Fig. 4:6 for the maximum value of S (the peak S_1) and theory for S_1 and the corresponding frequency N_1 versus range ρ. Figure 8 compares data of Fig. 4:10 for $P - 1$ vs $k\rho$ (for $\rho = 40$ and N varying from 4 to 20 in steps of 2) and corresponding theory versus $k\rho \approx 7.32N$. Figure 9 compares theory with data of Fig. 4:13 for P (at $\rho = 40$, and $N = 8$, 12, 16, 20) versus normalized receiver height $kZ_r/2\pi = 0.183NZ_r/2\pi$.

For Figs. 1–7, we take $h_t = h_r = 0.835$ corresponding to a tangent plane height 0.2 above the base plane plus the radius (0.635) of the microphone transducers resting on the tangent plane. For Fig. 8, associated with Fig. 4:10 for transducer faces parallel to the tangent plane ($Z_s = Z_r = 0$), we take the phase center heights as $h_t = h_r = 0.3$ (which gave better accord than 0.1, 0.2, or 0.4). For Fig. 9, we take $h_t = 0.3$ and $h_r > 0.3$.

The values of $C^2A \approx 2.42 \times 10^{-4}$ (in the radial loss exponent) and of $V_a \approx 0.2 - V \approx 0.097$ (the volume of air per unit area below the tangent plane) preserve the sequences in (1:53) and (1:54).

ACKNOWLEDGMENTS

Work supported, in part, by the Office of Naval Research and the National Science Foundation.

[1] R. J. Lucas and V. Twersky, "Inversion of data for near-grazing propagation over rough surfaces," J. Acoust. Soc. Am. **80**, 1459–1472 (1986); Suppl. 1 **79**, S68 (1986).
[2] R. J. Lucas and V. Twersky, "Coherent response to a point source irradiating a rough plane," J. Acoust. Soc. Am. **76**, 1847–1863 (1984); Suppl. 1 **74**, S122 (1983).
[3] H. Medwin, G. L. D'Spain, E. Childs, and S. J. Hollis, "Low-frequency grazing propagation over periodic steep-sloped rigid roughness elements," J. Acoust. Soc. Am. **76**, 1774–1790 (1984).
[4] H. Medwin and G. L. D'Spain, "Near-grazing, low-frequency propagation over randomly rough, rigid surfaces," J. Acoust. Soc. Am. **79**, 657–665 (1986).
[5] V. Twersky, "On scattering and reflection of sound by rough surfaces," J. Acoust. Soc. Am. **29**, 209–225 (1957); **22**, 539–546 (1950); J. Appl. Phys. **24**, 659–660 (1953).
[6] V. Twersky, "Reflection and scattering of sound by correlated rough surfaces," J. Acoust. Soc. Am. **73**, 85–94 (1983).
[7] I. Tolstoy, "Rough surface boundary wave attenuation due to incoherent scatter," J. Acoust. Soc. Am. **77**, 482–488 (1985); **72**, 960–972 (1982), **66**, 1135–1144 (1979).